Supporting Information

Both over 18.7% Efficiency of Bulk Heterojunction or Pseudo-planar Heterojunction Organic Solar Cells by Regulating the Intermolecular Compatibility

Zijian Zhang[a], Yu Zhang[a], Shixiu Sun[a], Hang Zhou[b], Jian Wang[*c], Yujie Xu[d], Xiaoyan Du[d], Sang Young Jeong[e], Han Young Woo[e], Fujun Zhang[*b] and Qianqian Sun[*a]

[a.] Collaborative Innovation Center of Light Manipulations and Applications in Universities of Shandong, School of Physics and Electronics, Shandong Normal University, Jinan 250014, China. E-mail: qianqiansun@sdnu.edu.cn

[b.] Key Laboratory of Luminescence and Optical Information, Ministry of Education, Beijing Jiaotong University, Beijing 100044, China. E-mail: fjzhang@bjtu.edu.cn

[c.] College of Physics and Electronic Engineering, Taishan University, Taian 271021, China. E-mail: wangjian@tsu.edu.cn

[d.] School of Physics State Key Laboratory of Crystal Materials, Shandong University, Jinan 250100, China.

[e.] Organic Optoelectronic Materials Laboratory, Department of Chemistry, College of Science, Korea University, Seoul 02841, Republic of Korea.

1. Experimental section

1.1 Device Fabrication:

The ITO glass substrates are sequentially pre-cleaned in the ultrasonic baths containing detergent, deionized water, or ethanol, respectively. The cleaned ITO substrate is blown-dried with nitrogen and treated with oxygen plasma for the 90s to improve work function and clearance. Subsequently, poly(3,4-ethylene dioxythiophene):poly(styrene sulfonate) (PEDOT:PSS, purchased from H.C. Starck Co. Ltd.) solution is spin-coated on ITO substrates at 5000 round per minute (RPM) for 30 s and dried at 150 ℃ for 10 minutes (min) in atmospheric air. Then ITO substrates coated with PEDOT:PSS films are transferred into a high-purity nitrogen-filled glove box. The active layer material used is purchased from Solarmer Materials Inc. Both the BHJ and PPHJ devices are fabricated with a conventional device structure of ITO/PEDOT:PSS/active layer/PDINN/Ag. For BHJ devices, the active layers are spin-coated from 17.6 mg/mL chloroform solution (D:A=1:1.2, 0.4 vol% DIO, with different weight ratios of BTP-eC9 in the acceptor mixture) at 3500 rpm for 40 s. For

PPHJ devices, firstly the donor layers are spin-coated from 8 mg/ml chloroform solution at 3300 rpm for 40 s. Then the acceptor layers are spin-coated from 9.6 mg/ml chloroform solution(0.4 vol% DIO, with different weight ratios of BTP-eC9 in the acceptor mixture) at 3500 rpm for 40 s on the top of the donor layers. Then, the active layers are annealed thermally annealed at 55 ℃ for 10 min. The methanol solution of PDINN (1.5 mg/mL) is spin-cast on the active layer at 3000 RPM for 30 s. Finally, a 100 nm Ag layer is thermally deposited under the vacuum condition of 7×10^{-5} Pa. The active area is approximately 3.8 mm^2, which is defined by the overlapping area of the ITO anode and Ag cathode.

1.2. Device characterization

The thicknesses of films prepared on the surface of ITO/PEDOT:PSS are measured by using an AMBIOS Technology XP-2 stylus profilometer. Absorption spectra of films are measured by using a PERSEE TU-1900 spectrophotometer. The contact angles of films are characterized by the Contact Angle meter. In-situ Photoluminescence Spectra Measurements are performed by the DU-200 dynamic spectrometer in transmission mode with a time interval of 0.05 s. The morphology images of films are characterized by an atomic force microscope (AFM, Horiba Bruker Multimode 8). The film-depth-dependent light absorption spectroscopy is acquired upon a film-depth-dependent light absorption spectrometer (PU100, Puguangweishi Co. Ltd). The current density-voltage (*J*–*V*) curves of the OSCs are measured under 1 sun AM 1.5 G illumination (100 mW cm^{-2}) in a high-purity nitrogen-filled glove box by using a Keithley 2400 source meter. The AM 1.5 G illumination is provided by XES-50S2 (SAN-EI Electric Co., Ltd.) solar simulator (AAA class, 40 × 40 mm^2 effective irradiated area). The external quantum efficiency (EQE) spectra of OSCs are measured by using a Zolix Solar Cell Scan 100 in atmospheric air. The photoluminescence (PL) spectra of BHJ films and PPHJ films with different ratios of BTP-eC9 are measured by a fluorescence spectrophotometer (FLS 1000). Electrochemical impedance spectroscopy (EIS) is measured in atmospheric air and dark conditions by an electrochemical workstation (CHI 760 E).

The measured contact angle values ϑ are input into the Wu model to calculate the polar surface energy (γ^p) and dispersive surface energy (γ^d) of films according to the following equation.

$$\gamma_W(1+cos\theta_W)=\frac{4\gamma_W^d\gamma^d}{\gamma_W^d+\gamma^d}+\frac{4\gamma_W^p\gamma^p}{\gamma_W^p+\gamma^p}$$

$$\gamma_{EG}(1+cos\theta_{EG}) = \frac{4\gamma_W^d\gamma^d}{\gamma_W^d+\gamma^d} + \frac{4\gamma_{EG}^p\gamma^p}{\gamma_{EG}^p+\gamma^p}$$

$$\gamma_W = \gamma_W^d + \gamma_W^p$$

$$\gamma_{EG} = \gamma_{EG}^d + \gamma_{EG}^p$$

$$\gamma^{tot} = \gamma^d + \gamma^p$$

W and EG refer to deionized water and ethylene glycol, ϑ_W and ϑ_{EG} are contact angle values of deionized water and EG is the probing liquids. γ_W and γ_{EG} are surface energy values of deionized water and EG. The total surface energy γ^{tot} is equal to the sum of γ^d and γ^p.

The calculated surface energy value is input into the Wu model to calculate the interfacial tension ($\gamma_{A/B}$) between A and B according to the following equation.

$$\gamma_{A/B} = \gamma_A + \gamma_B - 4\left(\frac{\gamma_A^d\gamma_B^d}{\gamma_A^d+\gamma_B^d} + \frac{\gamma_A^p\gamma_B^p}{\gamma_A^p+\gamma_B^p}\right)$$

The peak location and FWHM measured from GIWAX are entered into the following formula to calculate the d-spacing and CCL of the film.

$$d\ spacing = \frac{2\pi}{q}$$

$$CCL = \frac{2\pi k}{f_{whm}}$$

Where q is expressed as the peak location, k is the shape factor with a usual value of 0.9 and f_{whm} is the full width at the half maximum of the diffraction peak.

Carrier mobility is measured using the space-charge-limit current (SCLC) method. The electron mobility is determined with the device structure of ITO/ZnO/Active layer/PDINN/Al(100nm) and the hole mobility is determined with the device structure of ITO/PEDOT:PSS/Active layer/MoO_3/Ag(100nm). The devices are fabricated under optimized conditions. BHJ OSCs active layer films are prepared under the same conditions as PPHJ OSCs. The mobility is determined by fitting the dark current to the model of a single carrier SCLC, according to the equation:

$$J = \frac{9}{8}\varepsilon_r\varepsilon_0\mu\frac{V^2}{d^3}$$

where J is the current density, d is the film thickness of the active layer, μ is the charge carrier

mobility, ε_r is the relative dielectric constant of the transport medium, and ε_0 is the permittivity of free space. The ε_r parameter is assumed to be 3, which is a typical value for organic materials. In organic materials, charge mobility is usually field-dependent and can be described by the disorder formalism, typically varying with an electric field, $E = \frac{V}{d}$, according to the equation:

$$\mu = \mu_0 exp[0.89\gamma\sqrt{\frac{V}{d}}]$$

where μ_0 is the charge mobility at zero electric fields and γ is a constant. Then, the Mott-Gurney equation can be described by:

$$J = \frac{9}{8}\varepsilon_r\varepsilon_0\mu_0\frac{V^2}{d^3}exp[0.89\gamma\sqrt{\frac{V}{d}}]$$

In this case, the charge mobilities are estimated using the following equation:

$$\ln(\frac{Jd^3}{V^2}) = 0.89\gamma\sqrt{\frac{V}{d}} + \ln(\frac{9}{8}\varepsilon_r\varepsilon_0\mu_0)$$

The carrier mobility can be calculated from the slope of the curves.

2. Additional experimental results

Table S1. Summary of polar (γ^p) and dispersion (γ^d) components of surface tensions, surface tensions (χ), Flory-Huggins interaction parameters (γ) and Wetting coefficient (ω) for various films.

Surface	γ^p (mN m^{-1})	γ^d (mN m^{-1})	γ^{tot} (mN m^{-1})	χ		γ		ω_A
PM6	19.57	2.64	22.20	$\chi_{PM6:L8-BO}$	0.202	$\gamma_{PM6:L8-BO}$	0.591	/
L8-BO	22.27	4.37	26.64	$\chi_{PM6:BTP-eC9}$	0.378	$\gamma_{PM6:BTP-eC9}$	1.435	-0.24
BTP-eC9	22.18	5.96	28.14	$\chi_{L8-BO:BTP-eC9}$	0.020	$\gamma_{L8-BO:BTP-eC9}$	0.245	-2.01

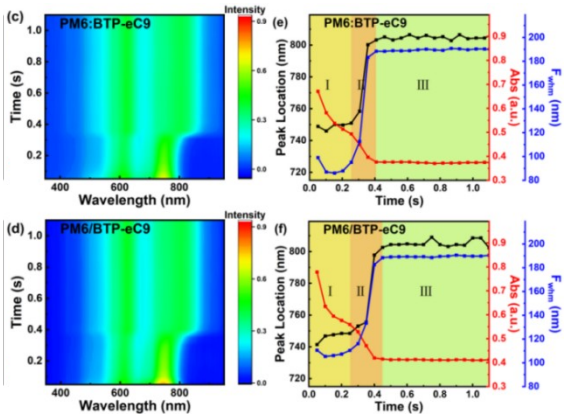

Figure S1. In-situ UV-vis absorption line profile of a) PM6:BTP-eC9 and b) PM6/BTP-eC9 film. Time-resolved UV-vis absorption spectra of c) PM6:BTP-eC9 and d) PM6/BTP-eC9 film. Time evolution of the peak position, intensity and FWHM for e) PM6:BTP-eC9 and f) PM6/BTP-eC9 film.

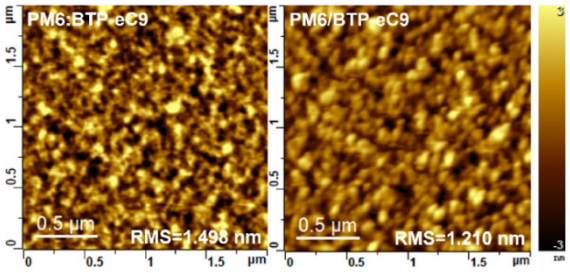

Figure S2. AFM images of the blend films.

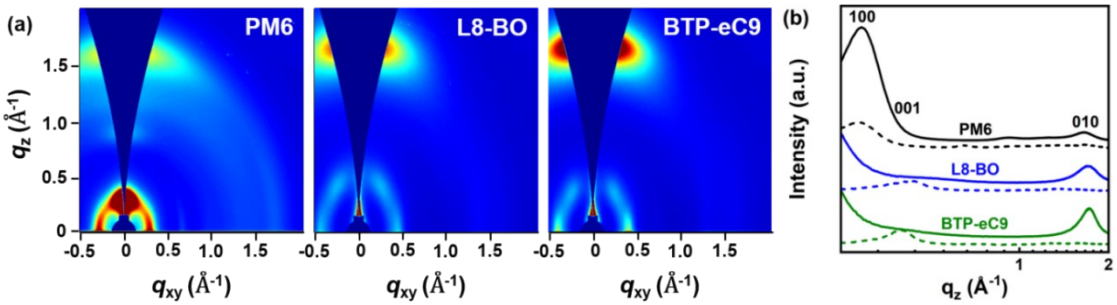

Figure S3. a) 2D GIWAXS images of pure films. b) Out-of-plane (solid lines) and in-plane (dotted lines) profiles abstracted from 2D GIWAXS images for the corresponding pure films.

Table S2. Related GIWAXS data for pure films.

Film	Peak in IP direction				Peak in OOP direction			
	Q (Å^{-1})	d-spacing (Å)	FWHM (Å^{-1})	CCL (Å)	Q (Å^{-1})	d-spacing (Å)	FWHM (Å^{-1})	CCL (Å)
PM6	0.29	21.82	0.13	42.52	1.66	3.78	0.45	12.51
L8-BO	0.44	14.44	0.20	27.99	1.71	3.67	0.38	15.04
BTP-eC9	0.40	15.75	0.12	47.52	1.72	3.66	0.28	20.12

Table S3. Related data of the (100) peak and the (010) peak for blend films.

Structure	Film	(100) peak in IP direction				(010) peak in OOP direction			
		Q ($Å^{-1}$)	d-spacing (Å)	FWHM ($Å^{-1}$)	CCL (Å)	Q ($Å^{-1}$)	d-spacing (Å)	FWHM ($Å^{-1}$)	CCL (Å)
BHJ	PM6:L8-BO	0.31	20.57	0.11	53.35	1.70	3.69	0.34	16.83
	PM6:L8-BO:BTP-eC9	0.31	20.57	0.10	59.52	1.71	3.67	0.31	18.18
	PM6:BTP-eC9	0.31	20.57	0.10	58.30	1.71	3.67	0.30	18.79
PPHJ	PM6/L8-BO	0.31	20.57	0.10	54.90	1.71	3.68	0.33	17.19
	PM6/L8-BO:BTP-eC9	0.30	20.72	0.09	61.47	1.72	3.66	0.30	18.72
	PM6/BTP-eC9	0.30	20.72	0.09	60.81	1.71	3.67	0.30	19.10

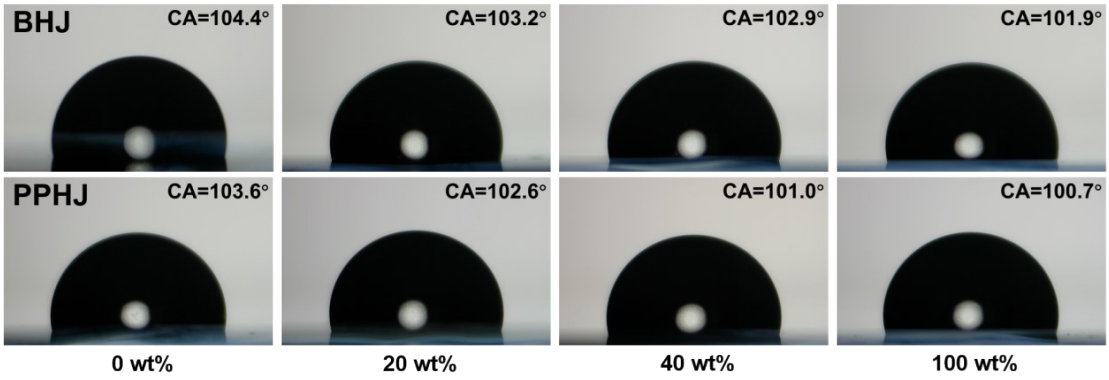

Figure S4. Water contact angle images of the ternary BHJ and PPHJ devices with different weight ratio of BTP-eC9 in the acceptor.

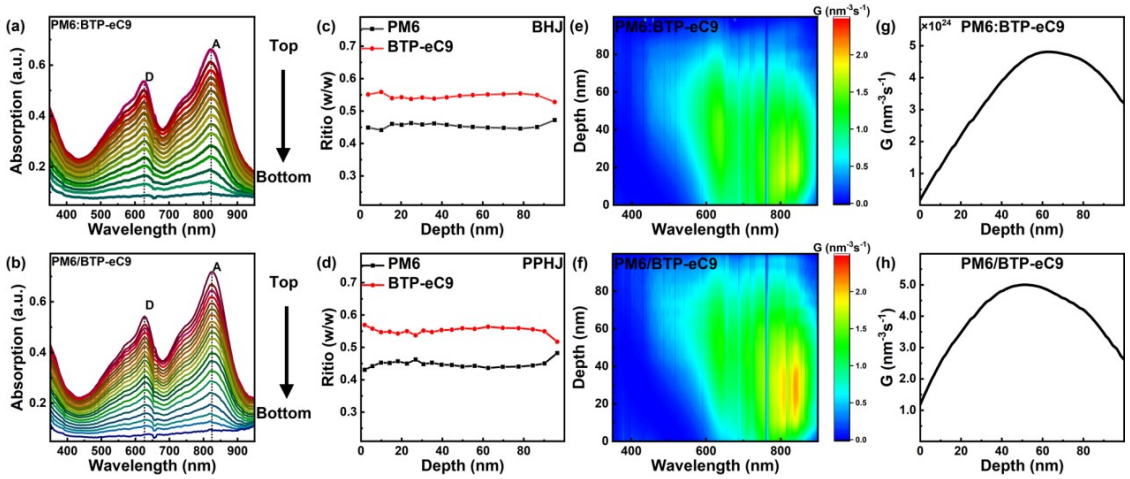

Figure S5. FLAS of a) PM6:BTP-eC9 and b) PM6/BTP-eC9 film, film-depth-dependent composition ratios of the donor and acceptor dependence on c) PM6:BTP-eC9 and d) PM6/BTP-eC9 film depth, exciton generation profile of e) PM6:BTP-eC9 and f) PM6/BTP-eC9 film, and G dependence on g)

PM6:BTP-eC9 and h) PM6/BTP-eC9 film depth.

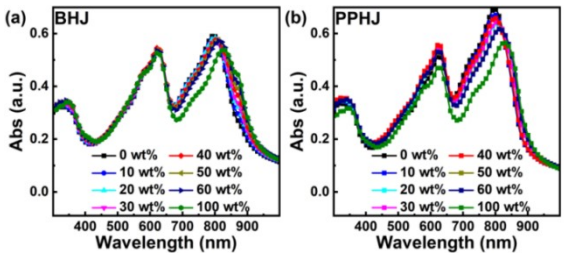

Figure S6. Absorption spectra of a) BHJ and b) PPHJ films.

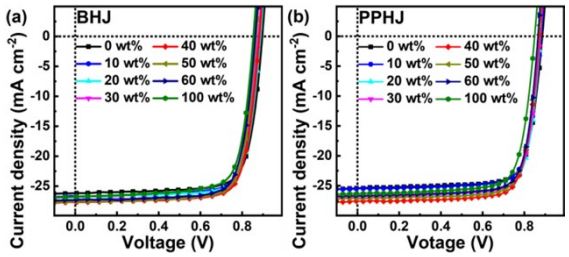

Figure S7. The *J*–*V* curves of OSCs with a) BHJ and b) PPHJ structure.

Table S4. Photovoltaic parameters of BHJ and PPHJ OSCs with different BTP-eC9 content.

Device type	BTP-eC9 (wt%)	V_{OC} (V)	J_{SC} (mA cm^{-2})	FF (%)	PCE (Ave.±Dev.) (%)
BHJ	0	0.90	26.15	75.65	17.82 (17.56±0.27)
	10	0.89	26.55	76.33	17.94 (17.68±0.26)
	20	0.89	26.75	76.41	18.06 (17.86±0.19)
	30	0.88	27.33	76.70	18.41 (18.15±0.25)
	40	0.88	27.68	77.48	18.92 (18.60±0.29)
	50	0.87	27.53	77.05	18.40 (18.36±0.22)
	60	0.87	27.06	76.88	18.10 (17.94±0.28)
	100	0.85	26.75	75.94	17.35 (16.97±0.32)
PPHJ	0	0.89	25.49	77.20	17.43 (17.16±0.27)
	10	0.88	25.81	77.44	17.51 (17.35±0.25)
	20	0.88	26.73	77.93	18.26 (18.00±0.24)
	30	0.88	26.86	78.02	18.44 (18.18±0.23)
	40	0.87	27.37	78.45	18.75 (18.52±0.21)
	50	0.87	26.99	78.13	18.29 (17.99±0.27)
	60	0.87	26.65	77.89	17.96 (17.67±0.27)
	100	0.85	26.29	76.93	17.18 (16.91±0.35)

The average and deviation values of PCEs are obtained from 10 individual cells.

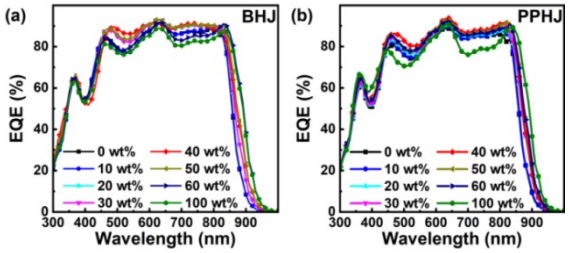

Figure S8. The EQE spectra of OSCs with a) BHJ and b) PPHJ structure.

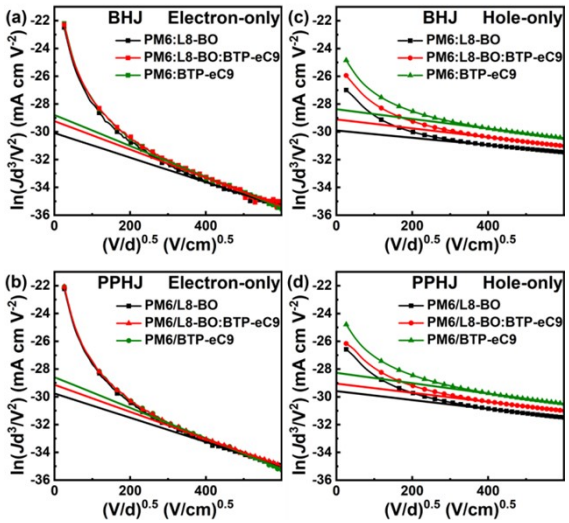

Figure S9. The $\ln(JL^3/V^2)$ versus $(V/L)^{0.5}$ curves of a) electron-only devices and c) hole-only devices with BHJ structure, b) electron-only devices and d) hole-only devices with PPHJ structure.

Table S5. The hole mobility (μ_h), electron mobility (μ_e) and μ_h/μ_e values in BHJ and PPHJ films.

Device type	BTP-eC9 (wt%)	μ_h ($cm^2\ V^{-1}\ s^{-1}$)	μ_e ($cm^2\ V^{-1}\ s^{-1}$)	μ_h/μ_e
BHJ	0	3.45×10^{-4}	2.85×10^{-4}	1.21
	40	7.69×10^{-4}	6.74×10^{-4}	1.14
	100	1.60×10^{-3}	1.05×10^{-3}	1.53
PPHJ	0	4.72×10^{-4}	3.98×10^{-4}	1.18
	40	8.10×10^{-4}	7.43×10^{-4}	1.09
	100	1.77×10^{-3}	1.28×10^{-3}	1.38

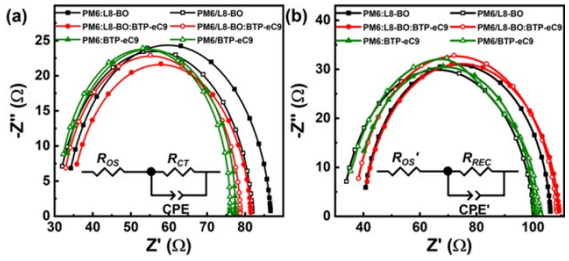

Figure S10. Nyquist plots of different OSCs in the a) light and b) dark.

Table S6. Fitted parameters of OSCs in BHJ and PPHJ active layers.

Device type	BTP-eC9 (wt%)	R_{OS} (Ω)	R_{CT} (Ω)	R_{REC} (Ω)
BHJ	0	32.65	54.09	66.39
	40	33.91	47.62	69.63
	100	31.99	45.37	63.99
PPHJ	0	30.31	51.65	68.13
	40	31.71	47.03	71.76
	100	31.07	44.89	66.43

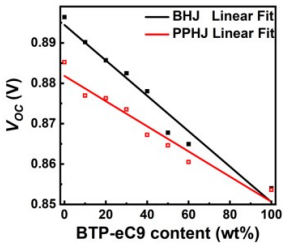

Figure S11. Correlation between BTP-eC9 content in acceptors and V_{OC} in BHJ and PPHJ OSCs.

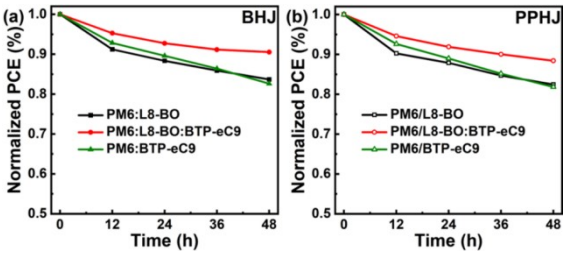

Figure S12. Normalized PCE plots of a) BHJ OSCs and b) PPHJ OSCs in the stability test of thermal aging by continuous heating unencapsulated devices at 60 °C for different time.